The MODIS Cloud Products: Algorithms and Examples From Terra

Steven Platnick, Michael D. King, *Member, IEEE*, Steven A. Ackerman, W. Paul Menzel, Bryan A. Baum, Jérôme C. Riédi, and Richard A. Frey

Abstract—The Moderate Resolution Imaging Spectroradiometer (MODIS) is one of five instruments aboard the Terra Earth Observing System (EOS) platform launched in December 1999. After achieving final orbit, MODIS began earth observations in late February 2000 and has been acquiring data since that time. The instrument is also being flown on the Aqua spacecraft, launched in May 2002. A comprehensive set of remote sensing algorithms for cloud detection and the retrieval of cloud physical and optical properties have been developed by members of the MODIS atmosphere science team. The archived products from these algorithms have applications in climate change studies, climate modeling, numerical weather prediction, as well as fundamental atmospheric research. In addition to an extensive cloud mask, products include cloud-top properties (temperature, pressure, effective emissivity), cloud thermodynamic phase, cloud optical and microphysical parameters (optical thickness, effective particle radius, water path), as well as derived statistics. We will describe the various algorithms being used for the remote sensing of cloud properties from MODIS data with an emphasis on the pixel-level retrievals (referred to as Level-2 products), with 1-km or 5-km spatial resolution at nadir. An example of each Level-2 cloud product from a common data granule (5 min of data) off the coast of South America will be discussed. Future efforts will also be mentioned. Relevant points related to the global gridded statistics products (Level-3) are highlighted though additional details are given in an accompanying paper in this issue.

Index Terms—Clouds, meteorology, remote sensing, satellite applications, terrestrial atmosphere.

I. INTRODUCTION

THE Moderate Resolution Imaging Spectrometer (MODIS), developed for the NASA Earth Observing System (EOS) Terra and Aqua satellites, provides an unprecedented opportunity for earth remote sensing. In particular, complete spectral coverage in key atmospheric bands has

S. Platnick is with the Laboratory for Atmospheres, NASA Goddard Space Flight Center, Greenbelt, MD 20771 USA (e-mail: steven.platnick@nasa.gov).

M. D. King is with the Earth Sciences Directorate, NASA Goddard Space Flight Center, Greenbelt, MD 20771 USA.

S. A. Ackerman is with the Department of Atmospheric and Oceanic Sciences, University of Wisconsin, Madison, WI 53706 USA.

W. P. Menzel is with the National Oceanic and Atmospheric Administration, National Environmental Satellite, Data, and Information Service, University of Wisconsin, Madison, WI 53706 USA.

B. A. Baum is with NASA Langley Research Center, Hampton, VA 23681 USA.

J. C. Riédi is with the Goddard Earth Sciences and Technology Center, University of Maryland—Baltimore County, Baltimore, MD 21228 USA.

R. A. Frey is with the Cooperative Institute for Meteorological Satellite Studies, University of Wisconsin, Madison, WI 53706 USA.

spurred the development of new spaceborne algorithms, while moderate but global spatial coverage (1 km or better at nadir) allows for the implementation of heritage algorithms at a higher spatial resolution than has previously been possible.

The Terra spacecraft was launched on December 18, 1999, with the first science data stream beginning on February 24, 2000. Since that time, many algorithms have undergone significant refinement and improvement. We report on the progress to date on the core MODIS cloud algorithms and give examples from Terra. These products include cloud detection and masking, cloud-top properties (pressure, temperature, effective emissivity), thermodynamic phase, and optical and microphysical properties (optical thickness, particle size, water path). The challenge of these algorithms is in providing retrievals on a global operational basis. That is, the algorithms are designed to operate over all ecosystems and under a variety of atmospheric conditions. The cloud products described in this paper are part of a suite of MODIS atmosphere products that are summarized in an accompanying paper in this issue [1]. The same cloud algorithms we describe in this paper will be used for MODIS on Aqua, launched in May 2002.

The salient features of the MODIS instrument have been described by a number of authors [2]–[4]. Only the most relevant characteristics will be mentioned in this paper. MODIS is a 36-channel whiskbroom scanning radiometer. The channels (referred to as "bands" in the MODIS nomenclature) are distributed between 0.415 and 14.235 μm in four focal plane assemblies, with nadir spatial resolutions of 250 m (two bands), 500 m (five bands), and 1000 m (29 bands). The 250-m bands are centered at 0.65 and 0.86 μm with the 500-m bands at 0.47, 0.56, 1.24, 1.63, and 2.13 μm. Each band's spectral response is determined by an interference filter overlying a detector array imaging a 10-km along-track scene for each scan (i.e., 40, 20, and 10 element arrays for the 250, 500, and 1000-m bands, respectively). MODIS has several onboard instruments for in-orbit radiometric and spectral characterization [5], [6]. Of particular importance to the cloud optical and microphysical algorithms, which are fundamentally based on solar reflectance values and not radiance, is a solar diffuser panel for reflectance calibration up through the 2.1-μm MODIS band and an accompanying diffuser stability monitor for assessing the stability of the diffuser up to 1 μm.

MODIS scans a swath width sufficient for providing global coverage every two days from a polar-orbiting, sun-synchronous platform at an altitude of 705 km. While Terra is in a descending orbit with an equatorial crossing of 1030 local solar time, Aqua is in an ascending orbit with a 1330 local crossing

TABLE I
SUMMARY OF MODIS PIXEL-LEVEL (LEVEL-2) CLOUD PRODUCTS AND THEIR CURRENT DEPENDENCIES. * TERRA DESIGNATION (AQUA IDs ARE MYD35, MYD06, ETC.); [a] NSIDC NISE AND/OR NCEP SEA ICE CONCENTRATION; [b] NCEP GDAS SIX-HOUR DATASET; [c] NCEP REYNOLDS BLENDED SST PRODUCT; [d] AGGREGATION OF MODIS ECOSYSTEM CLASSIFICATION PRODUCT (MOD12) WITH MODIS DIFFUSE SKY SURFACE ALBEDO PRODUCT (MOD43). SEE TEXT FOR FURTHER DETAILS

Retrieved parameter	Earth Science Data Designation Product ID*	Investigators	MODIS spectral bands used	Spatial resolution (km)	MODIS ancillary input	Non-MODIS ancillary input
CLOUD MASK	**MOD35**	Ackerman *et al.*	up to 20 bands, VIS thru IR	0.25, 1		snow/sea ice mask [a]
CLOUD PROPERTIES	**MOD06**					
CLOUD TOP PROPERTIES						
Cloud-top pressure (p_c), cloud-top temperature (T_c), effective emissivity (f_ε)		Menzel *et al.*	11 µm and CO_2 bands (31–36)	5	**MOD35**	model/assimilated T, p profiles [b], SST [c]
CLOUD OPTICAL AND MICROPHYSICAL PROPERTIES:						
Cloud optical thickness (τ_c), particle effective radius (r_e), water path		King *et al.*	VIS, NIR, SWIR, MWIR (bands 1, 2, 5, 6, 7, 20)	1	**MOD35, MOD06** (p_c, T_c), ecosystem + surface albedo[d]	snow/sea ice mask [a], model/assimilated T, p profiles [b], SST [c]
Thermodynamic phase (IR algorithm)		Baum *et al.*	8.5, 11 µm bands (bands 29, 31)	5		

time. The three-hour offset between morning and afternoon orbits allows for some characterization of diurnal patterns.

With the exception of a 250-m cloud mask, all cloud products are at a scale of 1 or 5 km. Though archived at their native resolution, bands with subkilometer resolution are also aggregated into 1-km equivalent pixels, then combined with the 29 1-km bands and archived in a common file. This calibrated file (designated as Level-1B [6]), with a 1-km equivalent spatial resolution for all bands, is the basic input for the 1-km and 5-km cloud algorithms. All MODIS atmosphere products are archived into two categories: pixel-level retrievals (referred to as Level–2 products) and global gridded statistics at a latitude and longitude resolution of 1° (Level–3 products). The Level-3 products are temporally aggregated into daily, eight-day, and monthly files containing a comprehensive set of statistics and probability distributions (marginal and joint).

This paper is intended as an overview of the Level-2 cloud products (Section II). We will emphasize the MODIS cloud mask, used to discriminate clear-sky pixels from clouds, and retrievals of cloud optical and microphysical properties from solar reflectance measurements, specifically cloud optical thickness and particle effective radius for both liquid water and ice clouds. Additional cloud properties derived from thermal infrared bands, including cloud-top pressure, temperature, emissivity, and thermodynamic phase, will also be described. An example of each Level-2 product will be shown for a common MODIS data granule (5 min of orbit data) off the coast of Peru and Chile in July 2001. Details of the common atmospheric Level-3 product design are described in a companion paper [1] along with examples for the cloud products. In Section III we summarize relevant Level-3 issues.

II. PIXEL-LEVEL CLOUD PRODUCTS

We begin with a discussion of the MODIS cloud mask, which serves as the primary ancillary input to the other algorithms (Table I). We then proceed to cloud-top properties and thermodynamic phase. Results from each of these algorithms are required by the optical and microphysical product, which is discussed last. A granule of Terra MODIS data (July 18, 2001, 1530 UTC) is used as a common example for each product. A true-color composite image of the granule is shown in Fig. 1. The image shows extensive marine stratocumulus boundary layer clouds off the coasts of Peru and Chile. This stratocumulus regime is similar in nature to those off the west coasts of California and Namibia/Angola. In each case, the stratocumulus is caused by cool upwelling ocean water associated with coastal currents and the presence of high-pressure subsidence aloft [7]. Land-based clouds are evident in the image as well, overlying a wide variety of surfaces, including coastal deserts, high-altitude ecosystems, and low-land rain forests. The bright feature in southwest Bolivia (20.5 S, 67 W) is not a cloud but the high-altitude Uyuni Salt Flat (3700 m), one of the largest salt pans in the world. The pan is not correctly identified by either the cloud mask or the MODIS ecosystem product (used for surface albedo characterization as discussed in Section II-D.2).

MODIS data are stored in the Hierarchical Data Format (HDF) (cf., *hdf.ncsa.uiuc.edu*). Within this HDF file, each product has an associated Science Data Set (SDS) name. For example, the cloud-top pressure product is given the SDS name "Cloud_Top_Pressure", and for Terra is stored in the HDF data designation file "MOD06_L2" (which contains all Level-2
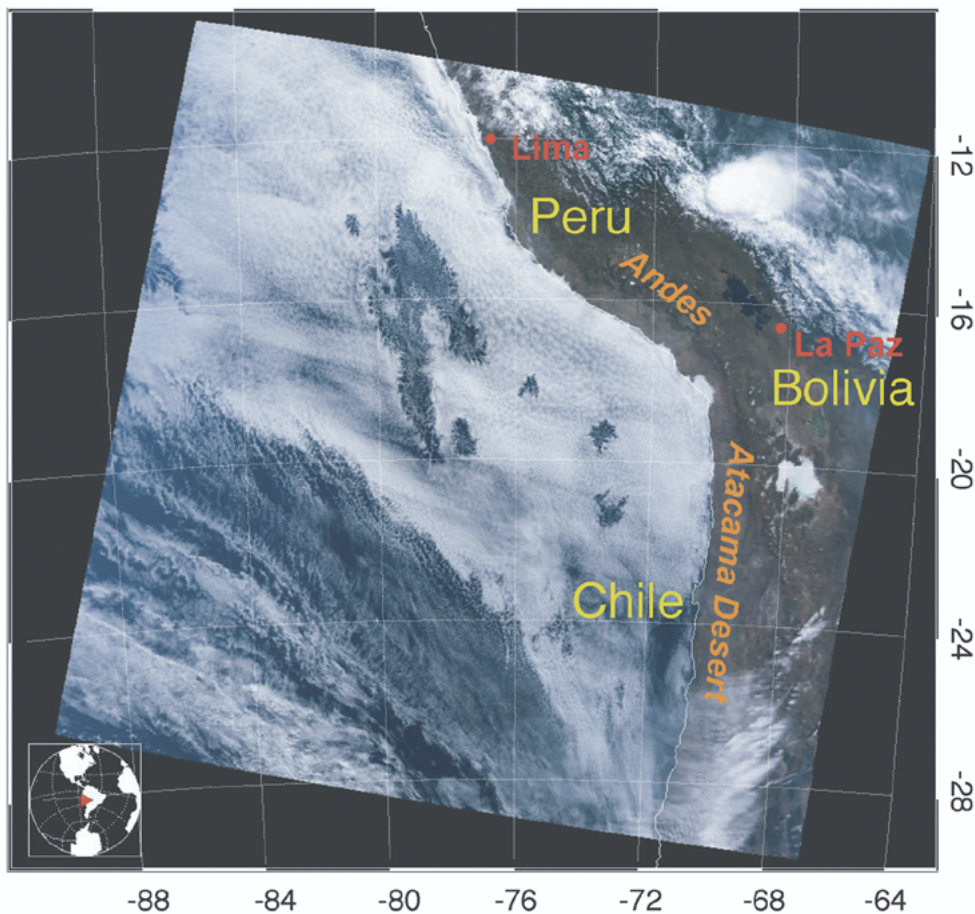
Fig. 1.   True-color composite of a granule of Terra MODIS data from July 18, 2001, 1530 UTC. The image shows widespread boundary layer stratocumulus clouds off the coasts of Peru and Chile, associated with cool upwelling water along the Humboldt current.

cloud-top property and optical/microphysical retrieval SDS's). Similarly, cloud mask results are found in the "MOD35_L2" HDF file (see Table I). Aqua products are designated with an "MYD" prefix. These ubiquitous HDF identification names are needed in accessing the archived products and are referred to in the literature as well. Both MOD06 and MOD35 Level-2 files contain geometry and geolocation data for every fifth pixel. A summary of file formats and specifications for all MODIS atmosphere products can be found at *modis-atmos.gsfc.nasa.gov*.

A. Cloud Detection and Masking

The MODIS cloud mask uses a variety of cloud detection tests to indicate a level of confidence that MODIS is observing a clear-sky scene. Produced globally day and night, at a 1-km pixel resolution, the cloud mask algorithm uses as many as 20 of the MODIS 36 spectral bands to maximize reliable cloud detection. A mask derived from the two 250-m resolution bands (0.65 and 0.86 μm) in combination with the 1-km cloud mask results is also produced and archived, but will not be discussed here.

The cloud mask essentially assesses the likelihood of a pixel being obstructed by clouds. As cloud cover can occupy a pixel to varying extents, the MODIS cloud mask is designed to allow for varying degrees of clear-sky confidence, i.e., it provides more information than a simple yes/no decision. To assist users in interpreting the results, the cloud mask consists of 48 bits of output per pixel that includes information on individual cloud test results, the processing path, and ancillary information (e.g., land/sea tag). In addition, the first eight bits of the cloud mask provide a summary useful for most applications. Further, the first two bits of the mask summarize the results from all individual tests by classifying cloud contamination in every pixel of data as either *confident clear*, *probably clear*, *uncertain/probably cloudy*, or *cloudy*.

The MODIS cloud mask algorithm identifies several conceptual domains according to surface type and solar illumination including land, water, snow/ice, desert, and coast for both day and night. Once a pixel is assigned to a particular domain (defining an algorithm path), a series of threshold tests attempt to detect the presence of clouds, or optically thick aerosol, in the instrument field of view (FOV). Each cloud detection test returns a confidence level that the pixel is clear ranging in value from one (high confidence clear) to zero (low confidence clear). There are several types of tests, with detection of different cloud conditions relying on a different combination of tests. Tests capable of detecting similar cloud conditions are grouped together. While these groups are arranged so that independence between them is maximized, few, if any, spectral tests are completely independent. As described in [8], a minimum confidence is determined for each group as follows:

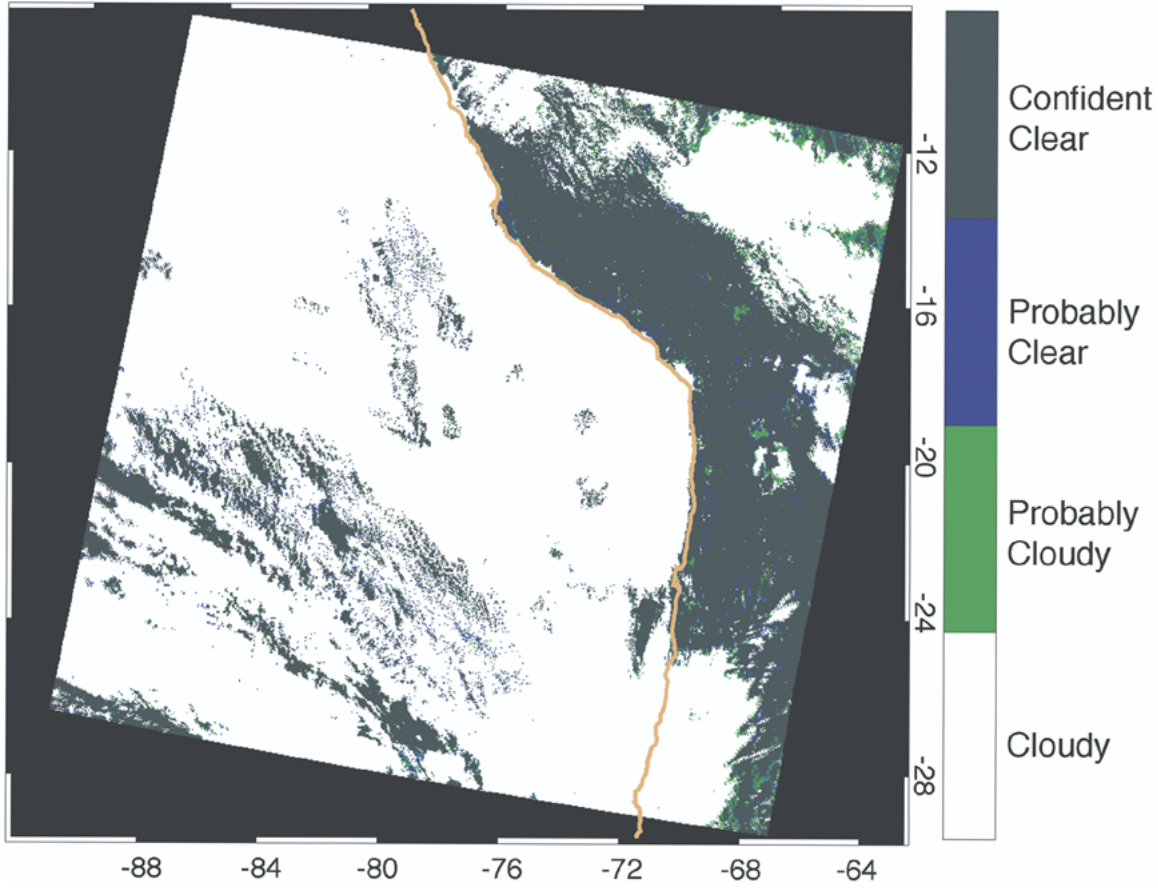$$G_{j=1,N} = \min\left[F_i\right]_{i=1,m} \tag{1}$$

Fig. 2.   The overall assessment from the MODIS cloud mask for the image of Fig. 1 as given by the first two bits of the mask.

where F_i is the confidence level of an individual spectral test, m is the number of tests in a given group, j is the group index, and N is the number of groups (e.g., 5). The final cloud mask confidence (Q) is then determined from the product of results for each group,

$$Q = N\sqrt[N]{\prod_{i=1}^{N} G_j}. \qquad (2)$$

This approach is clear-sky conservative in the sense that if any test is highly confident that the scene is cloudy $(F_i = 0)$, the final clear-sky confidence is 0. The four confidence levels included in the cloud mask output are: 1) *confident clear* $(Q > 0.99)$; 2) *probably clear* $(Q > 0.95)$; 3) *uncertain/probably cloudy* $(Q > 0.66)$; and 4) *cloudy* $(Q \leq 0.66)$. These outcomes constitute the first two bits of the mask. Note that the result gives the confidence, or lack thereof, in the existence of a clear pixel and not the confidence in the presence of an overcast cloudy pixel. As such, the *cloudy* outcome can alternately be labeled as *not clear* (i.e., high confidence in an obstruction in the FOV). The distinction is important for subsequent cloud retrievals as will be discussed in Section II-D.

An image corresponding to these four outcomes is shown in Fig. 2 for the MODIS granule of Fig. 1. Most of the scene is assessed as being *confident clear* or *cloudy*. The relatively small proportion of *uncertain/probably cloudy* pixels generally lie near cloud edges as might be expected, and more frequently for land pixels due to reduced certainty in surface characteris-

tics. Pixels designated as *probably clear* tend to be small isolated regions over land, away from cloud edges.

A number of ancillary sources are used in processing the cloud mask (Table I). For surface snow and ice, these include the Near Real-Time Ice and Snow Extent (NISE) [9] product from the National Snow and Ice Data Center, and the NOAA National Centers for Environmental Prediction (NCEP) $0.5°$ resolution sea ice concentration product [10].

Cloud masking is inherently more difficult over nonvegetated surfaces, transitional areas between desert and vegetated surfaces, high-elevation regions (e.g., mountains, Antarctica plateau), in sunglint regions, and nighttime masking in the presence of strong surface temperature inversions. Improvements to the mask have been made to correct for the high-elevation problem and are being developed for the others issues as well. Future efforts will also address ecosystem-specific improvements, improved discrimination for boundary layer cumulus clouds, and the nighttime algorithm.

B. Cloud Top Properties: Pressure, Temperature, Effective Emissivity

The CO_2 slicing technique to infer cloud-top pressure and effective cloud amount or emissivity (product of cloud fraction and cloud emissivity at 11 μm) has been discussed in detail in [11] and [12]. The method takes advantage of differing partial absorption in several of the MODIS infrared bands located within the broad 15-μm CO_2 absorption region, with each band being sensitive to a different level in the atmosphere. Clouds
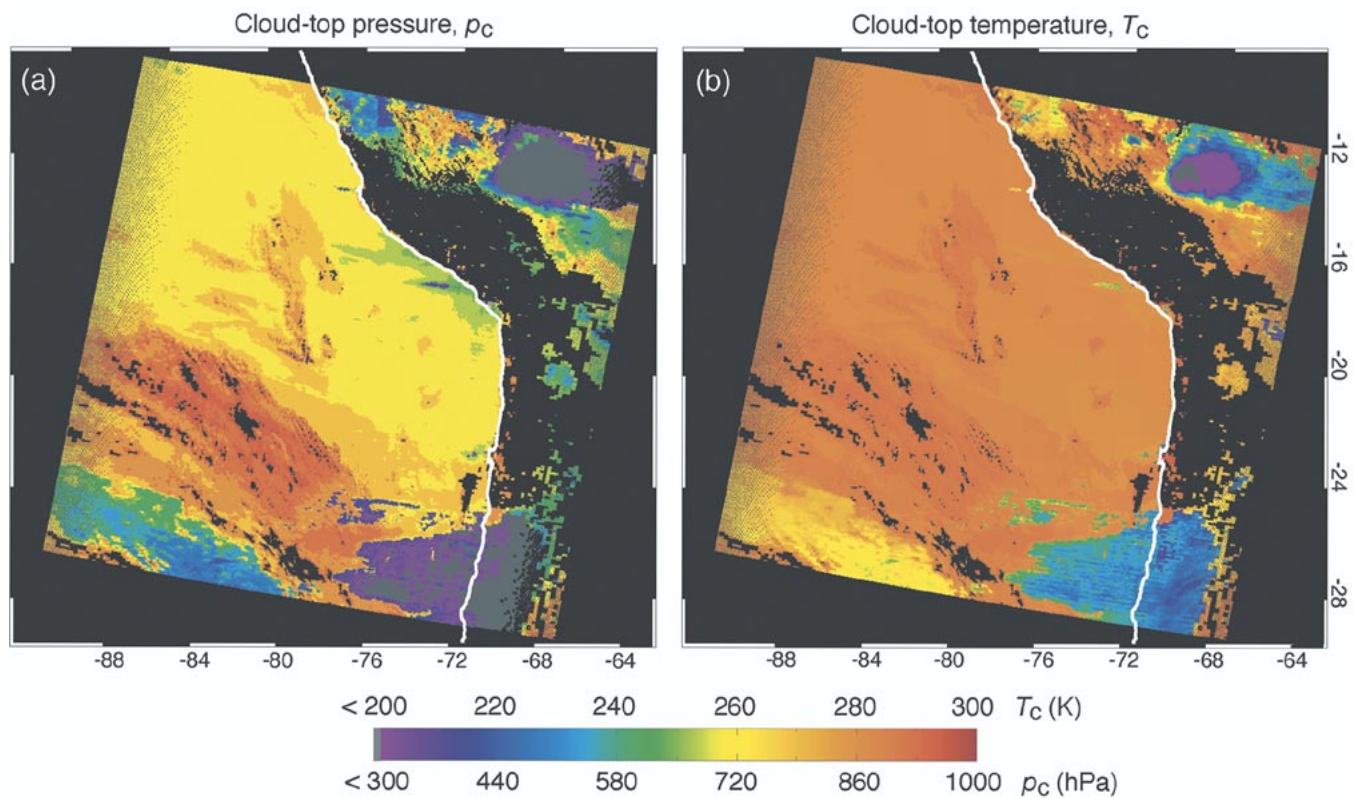
Fig. 3.   (a) Cloud-top pressure and (b) temperature retrievals for the image of Fig. 1.

appear in the CO_2-band images according to their level in the atmosphere. Low clouds will not appear at all in the high-absorptions bands, while high clouds appear in all bands. By measuring upwelling infrared radiation from the earth-atmosphere system in several of the MODIS CO_2 bands simultaneously, it is possible to infer the cloud-top pressure independently of the effective cloud amount. The CO_2 slicing technique has the ability to retrieve cloud pressure and effective cloud amount for opaque or nonopaque mid- to high-level clouds [11]. Cloud height accuracy increases as the observed cloud signal (the clear sky minus the measured radiance) increases for a FOV. For clouds at pressures greater than 700 hPa (i.e., close to the surface), the cloud signal decreases, thereby precluding application of the method. For low-level clouds, the infrared window 11-μm band temperature is used to determine a cloud-top temperature assuming the cloud is optically thick, and a cloud-top pressure is assigned by comparing the measured brightness temperature to the NCEP Global Data Assimilation System (GDAS) temperature profile [13].

Retrievals are derived from ratios of differences in radiances between cloudy and clear-sky regions at two nearby wavelengths. Error analyses for the method are provided in [14]–[16]. The method has been used in operational processing of GOES (Geostationary Operational Environmental Satellite) and HIRS (High resolution Infrared Radiometer Sounder) data, and has been found to have accuracies of approximately 50 hPa for clouds at heights above 3 km (approximately 700 hPa).

With the four MODIS sounding channels and the 11-μm window band, it is possible to determine a number of separate cloud-top pressures and effective cloud amounts. In MODIS operational processing, cloud-top pressures are calculated for

the following ratio pairs: 14.2 μm/13.9 μm; 13.9 μm/13.6 μm, 13.6 μm/13.3 μm, 13.9 μm/13.3 μm, and 13.3 μm/11 μm. The emission and absorption of the cloud are assumed to be identical in the spectral band pairs. Previous studies have not included the 13.3-μm/11-μm-band pair, but its use is restricted to ice cloud only. The most representative cloud pressure is chosen by minimizing the difference between the observed cloud signal and the cloud signal calculated from a forward radiative transfer model [11].

The fundamental CO_2 slicing retrievals are pressure and effective emissivity applied to a 5×5 pixel scene (5-km spatial scale at nadir). The algorithm currently uses modeled/assimilated analyses from the GDAS gridded meteorological profile product ($1°$, six hours instantaneous spatial/temporal resolution) [13], and the NCEP Reynolds Blended Sea Surface Temperature (SST) product [17]. The required clear-sky radiances are calculated from this dataset. Once the cloud-top pressure is determined for a given 5×5 scene, cloud-top temperature may readily be determined from the corresponding temperature profile. The MODIS cloud mask is used by the cloud-top property algorithm (Table I). Of the 25 pixels, at least four must be flagged as *probably cloudy* or *cloudy* by the cloud mask. The algorithm is run for both day and night observations.

The cloud-top pressure and temperature retrievals for the granule of Fig. 1 are shown in Fig. 3(a) and (b). Marine stratocumulus cloud tops are relatively warm and low ($p_c \sim 720$ hPa, $T_c \sim 280$ K). Higher/colder clouds are seen to the south, with especially strong convective activity over the Amazonian basin toward the northeast ($p_c < 300$ hPa, $T_c < 200$ K in the convective core). One may note that the cloud altitude decreases as the marine stratus cloud fraction decreases. For
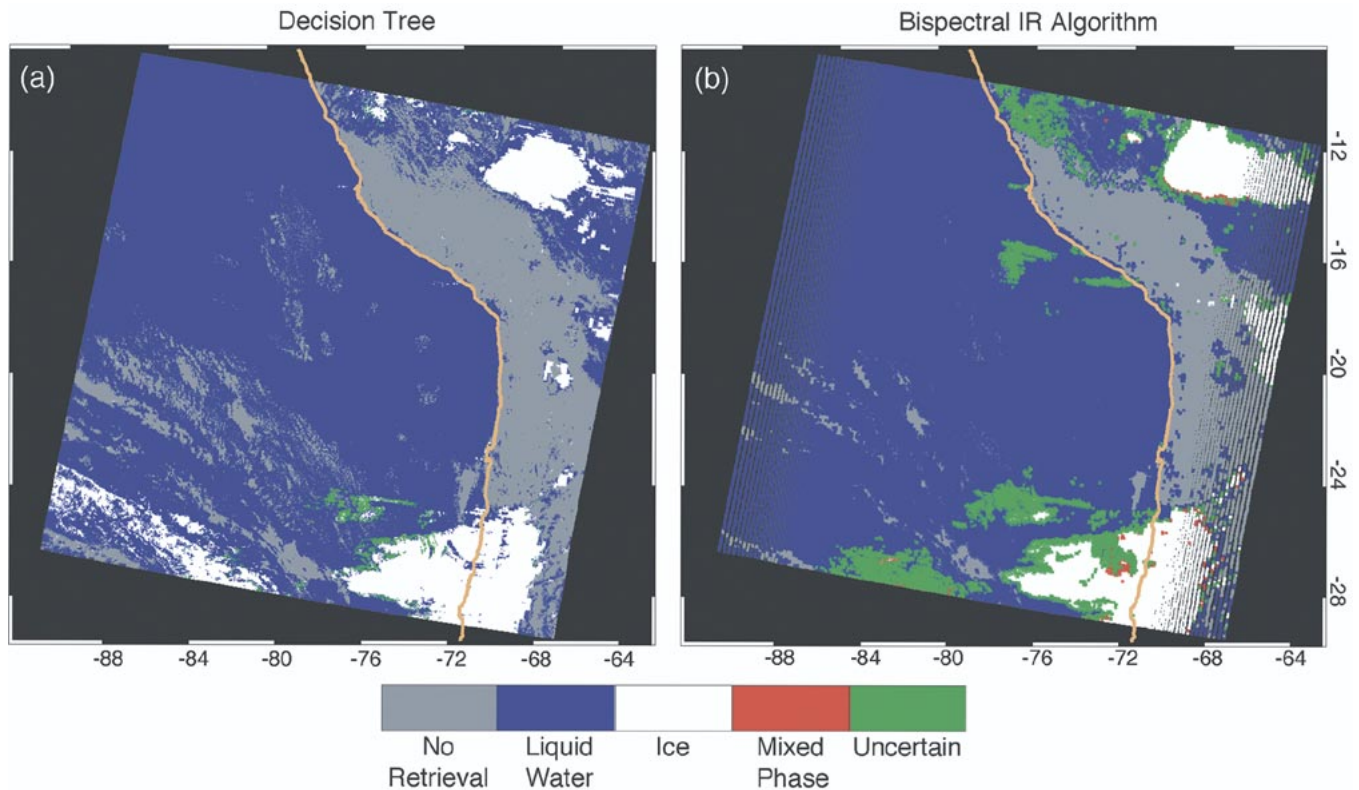
Fig. 4.   Two methods for inferring cloud thermodynamic phase. (b) Results from the bispectral IR algorithm (8.5- and 11-μm MODIS bands). The logic of the "decision tree" in (a) is based on results from individual cloud mask tests, the IR and SWIR phase algorithms, and cloud-top temperature retrievals. The decision tree inference is on a 1-km scale while the IR retrieval is at 5 km. The speckled appearance near the scan edge of the IR retrieval image is an artifact of insufficient interpolation to 1-km scales.

these low-level clouds, the 11-μm brightness temperatures are used to infer cloud temperature under the assumption that the cloud is opaque, as stated earlier in this section. This is a case where the low cloud is likely nonopaque within the 5×5-km region, resulting in a positive cloud-top temperature bias.

Future cloud-top retrieval efforts will include estimation of clear-sky radiance biases and corrections. Given a best estimate of the atmospheric state (from a global analysis or a forecast model), it is found that forward calculations of the radiances are different from those actually observed. The differences can be attributed to MODIS calibration errors (including knowledge of spectral response functions), inaccuracies in the estimation of the atmospheric state, or inadequacy in the forward model. Regardless of the cause, when comparing differences of clear (calculated) and cloudy (observed) radiances to infer cloud-top pressures with the CO_2 slicing algorithm, it is necessary to adjust for the radiance bias between calculated and observed radiances. This should be done using the clear-sky radiance composite from the last several days to assure good global coverage. To date these composites have not been available in a timely fashion, so radiance bias adjustments are still pending.

C. Cloud Thermodynamic Phase

There are currently three inferences of cloud phase archived in the MODIS cloud product (archived into the same product ID designation; see Table I). First, a bispectral infrared (IR) algorithm uses the inherent difference in water and ice optical constants (SDS "Cloud_Phase_Infrared"). A second algorithm is based on optical constant differences between water and ice

in selected shortwave IR (SWIR) bands (1.6, 2.1 μm). Finally, a logic-based "decision tree" that uses results from individual cloud mask tests (those containing both height-based and optical constant information) as well as IR, SWIR, and cloud-top temperature retrievals was developed specifically for the optical thickness and microphysical retrieval algorithm (to be discussed further in Section II-D). Results from the latter two phase algorithms are not stored as an SDS but are part of the 1-km pixel-level QA (see Section II-D.1). We discuss the IR-based bispectral algorithm in this section: the decision tree logic will be discussed in Section II-D.1.

The basis for the inference of cloud phase from the 8.52- and 11-μm bands is the difference of microphysical and optical properties between water droplets and ice crystals [18], [19]. Radiative transfer simulations (following [19], [20]) indicate that the brightness temperature difference between the 8.5- and 11-μm bands (hereafter denoted as $\mathrm{BTD}\{8.5–11\}$) tends to be positive for ice clouds that have a visible optical thickness greater than approximately one. Water clouds of relatively high optical thickness tend to exhibit negative $\mathrm{BTD}\{8.5–11\}$ values less than -2 K. The calculations showed that the $\mathrm{BTD}\{8.5–11\}$ values are quite sensitive to atmospheric absorption, especially water vapor. The BTD value for lower clouds tends to become more negative as the water vapor loading increases, and also as the surface emittance at 8.5 μm decreases. While a relatively small effect, multiple scattering was included in radiative transfer simulations of $\mathrm{BTD}\{8.5–11\}$. As with any IR technique, the $\mathrm{BTD}\{8.5–11\}$ approach can be used for both daytime and nighttime retrievals.

The IR phase retrieval is shown in Fig. 4(b). The algorithm is currently being run at a 5-km scale (average of 5×5 pixels) but is being considered as a 1-km product. It is being run on both day and night observations. As with cloud-top properties, four of the 25 pixels must be flagged by the cloud mask as *probably cloudy* or *cloudy* for the retrieval to proceed. Possible outcomes are: *uncertain phase*, *mixed phase*, *ice*, or *liquid water*. The marine stratus region is classified as being mostly composed of water at cloud-top, while areas of convection in the upper- and lower-right portions of the image are classified as being ice. In the lower-right region, however, there is some indication that cirrus is spreading to the west from the area of active generation over land. Inspection of various spectral bands (e.g., 1.38-μm band with strong water vapor absorption obscuring low clouds) tends to reinforce the idea that the cirrus is overlying a water cloud stratus deck. This raises the issue of how multilayered clouds can cause confusion for retrieval methods that assume a single cloud layer within any individual FOV. A case in point occurs in the region near ($\sim 25^{\circ}$S, 76°W), where there is some flagging of high clouds by the cloud-top property algorithm [Fig. 3(a)] but not over an area as extensive as that indicated by Fig. 4(b). In this region, spectral imagery indicates that optically thin cirrus is present over the boundary layer cloud. The cloud phase classification generally returns an *uncertain* or *mixed phase* in this situation.

There are several outstanding issues. For example, phase discrimination for optically thin cirrus remains problematic. Considerable effort is underway to improve the performance of the IR phase algorithm when optically thin ice clouds are present, regardless of surface type or solar illumination conditions. Another issue is the determination of the most prevalent cloud phase when the cloud-top temperature ranges from 233–273 K. In this temperature range, a mixture of both liquid and ice particles may be present. As supercooled water drops are prevalent over large areas in both hemispheres at higher latitudes, this is an important area that needs further investigation. An effort is underway to supplement the IR-based method with visible and near-infrared bands during daytime viewing conditions to improve the phase classification under these conditions.

D. Cloud Optical and Microphysical Properties

Cloud optical thickness (vertical integration of extinction over cloud physical thickness) and particle size are important in the radiative characterization and parameterization of clouds. In particular, it is the effective radius (defined as ratio of the third moment of size distribution to the second moment) that is the relevant weighting over the cloud particle size distribution for radiative transfer calculations. The retrieval of both quantities (hereafter simply referred to as a cloud retrieval) from simultaneous cloud reflectance measurements in various solar bands has been well studied in both theory and practice [21]–[28]. Useful spectral bands include window regions in the visible and near-infrared (allowing for conservative photon scattering with water particles), as well as the 1.6- and 2.1-μm shortwave infrared (SWIR) bands and the 3.7-μm midwave infrared band (MWIR) windows (progressively more absorption with increasing wavelength). While each of the three SWIR/MWIR bands is useful for particle size retrievals, an incomplete set

has been available for satellite observations prior to MODIS. For example, the widely used Advanced Very High Resolution Radiometer (AVHRR) on the NOAA polar orbiters is limited to a 3.7-μm band for cloud particle size retrievals [22], [25], [26]. A similar situation has existed for airborne imagery with the exception of the MODIS Airborne Simulator [27], [28] flown on the NASA high-altitude ER-2 aircraft.

All MODIS cloud microphysical and optical property retrievals are at 1 km. The retrievals are based on library calculations of plane-parallel homogeneous clouds overlying a black surface in the absence of an atmosphere. Separate libraries exist for liquid water and ice clouds, the latter consisting of 12 size distributions composed of four habits (aggregates, bullet rosettes, hollow columns, and plates) with the fraction of each habit depending on particle size. For example, the majority of large ice particles are assumed to be rosettes and aggregates. The habits are based on in situ observations from the FIRE-II experiment. Scattering calculations were made using the techniques of Yang and Liou [29], [30]. Surface albedo effects and corrections for nonunity atmospheric transmittance are accounted for on a pixel-by-pixel basis. Further detail follows.

1) To Retrieve or Not to Retrieve (and If So, What Phase?): In general, it is more straightforward to determine that a pixel is clear of clouds than it is to assess the likelihood of the opposite situation, i.e., that a pixel is completely overcast. It is the latter information that is needed for the cloud retrievals discussed in this section, while the MODIS cloud mask provides the former. A *not clear* outcome given by the first two bits of the mask does not necessarily mean that a pixel is suitable for a retrieval of optical thickness and particle size since the algorithm assumes an overcast scene. Note that the 5-km scale cloud-top property retrievals discussed in Section II-B were not as sensitive to this issue as the algorithm inherently accounts for nonunity cloud fraction within the 5-km scene through the effective emissivity parameter.

Two preliminary pieces of information are required by the algorithm: 1) An assessment of whether a pixel is suitable for performing a cloud retrieval (i.e., overcast), and 2) an estimate for the appropriate thermodynamic phase of the cloud. With regard to phase, it is recognized that multilayer clouds of different phases or mixed phase clouds are not only possible, but common. Therefore, since only a single phase is considered in the algorithm, the appropriate phase depends on the spectral bands being used. For example, a wavelength with little absorption (e.g., in the visible) may penetrate a thin cirrus layer to a lower level water cloud and contain information predominantly characteristic of water droplets. Alternatively, a more absorbing wavelength for ice (e.g., 3.7 μm) may show predominantly ice particle scattering characteristics.

A logical decision tree was developed to address both of the above needs. The decision tree is based on individual cloud mask tests coupled with IR, SWIR, and cloud-top temperature retrievals. The decision tree logic is modified according to the general underlying surface ecosystem (ocean, land, desert, coastal, snow/ice). For all ecosystems, only pixels with the cloud mask's two highest confidence cloudy bits are considered for processing. We discuss the remaining decision tree logic through an example.

Over the ocean, a combination of two cloud mask tests (1.38-μm reflectance and BT11-BT3.7) are used to initially decide whether a cloudy pixel consists of liquid water. Small 1.38-μm reflectance is indicative of low cloud while water clouds will be more reflective at 3.7 μm relative to ice clouds that have greater particle absorption at that wavelength. The tests are therefore a combination of altitude and particle index of refraction (3.7 μm). If both tests suggest the liquid water phase, then the pixel is flagged as such. Otherwise, the water phase is ruled out with the remaining possibilities being ice or uncertain phase. When the 1.38-μm test is not run (over high-altitude land regions including Greenland, Antarctica, and mountainous regions), only the BT11-BT3.7 test is used. Two remaining cloud mask tests are evaluated, making use of the 6.7-μm water vapor band and the 1.38-μm band. If either indicates a high cloud, then the pixel is flagged as ice; otherwise the phase is considered uncertain.

Whenever this initial application of cloud mask tests yields an uncertain phase, the result of the IR phase retrieval is used instead. An uncertain designation in the IR retrieval is left alone; mixed phase is changed to ice. Two additional tests are then applied to all pixels. The SWIR phase retrieval, using reflectance ratios of the 1.6- and/or 2.1-μm band reflectance to the 0.67-μm band, is applied first. Reflectance ratios greater or smaller than a predetermined range of values indicate water and ice, respectively, and previous assignments from the cloud mask and IR phase algorithm are overwritten accordingly. Pixels with intermediate reflectance ratios are unchanged. Finally, cloud-top temperature is used as a final check; pixels with values less than 233 K are set to ice, those greater than 273 K are set to water. Due to inherent biases in the logic, any remaining uncertain phase pixels are processed as water.

A difficult situation arising with water surfaces is the possibility of sunglint contamination. The cloud mask algorithm defines the potential geometric suglint region as being within 36° of the specular direction; the actual glint geometry will depend on surface wind speed and geometry. Within this potential glint region, cloud mask spectral reflectance tests are modified to minimize clear-sky sunglint observations from being erroneously flagged as cloud. In keeping with the clear-sky conservative design of the mask, the emphasis is in accurately identifying clear pixels and not overcast pixels. As a result, the ability to unambiguously identify cloudy pixels relative to pixels away from sunglint is reduced. In practice, it was found that use of the two highest confidence cloudy bits in the decision tree caused sunglint in large regions of the tropics (e.g., Indian Ocean) to be processed as clouds. Restricting the retrieval choice to only the highest confidence cloudy bit improved the situation, but at the expense of eliminating cloudy pixels in other sunglint regions. The current implementation of the algorithm uses this more conservative approach for observations within the sunglint geometry. A modification to the cloud mask in the glint region, where test thresholds are a function of angle away from the specular direction, is being implemented into the latest production version of the mask.

The decision tree phase inference is shown in Fig. 4(a). There is general agreement with the IR algorithm, though less cloud is flagged as uncertain as a result of the SWIR ratio tests. In par-

ticular, the thin cirrus overlying the lower stratocumulus water cloud is now flagged as liquid, indicating that the cirrus had relatively little effect on the SWIR reflectance. As previously mentioned, the concept of a single unambiguous phase for mixed-phase or multilevel clouds is problematic and is likely to depend on the spectral band considered. So while liquid water is deemed a more appropriate choice for the SWIR-based retrieval, a thermal emission technique might correctly consider this region to be ice or uncertain. The geometric sunglint region in this data granule is at the northern extreme (not over water) and therefore not a factor.

The decision tree phase inference is archived as part of the pixel-level runtime Quality Assessment (QA) information. The QA constitutes a separate Science Data Set (SDS) within the MOD06_L2 HDF data file (Section II). The QA associated with the 1-km cloud optical/microphysical portion of MOD06 is named "Quality_Assurance_1km"; likewise, QA associated with the 5-km cloud-top properties product are in the "Quality_Assurance_5km" SDS. QA runtime flags include product quality as well as processing path information. The phase used in the processing of each pixel is reported in the "Quality_Assurance_1km" SDS.

2) Surface Albedo: Cloud reflectance over land may be significantly affected by the underlying surface albedo, which is highly variable spectrally and with surface type. The MODIS surface spectral BRDF/albedo product MOD43 [31] provides 16-day 1-km composites of clear-sky observations for both bidirectional reflectance and albedo (solar illumination and diffuse sky) in most MODIS solar bands used in the cloud retrieval algorithm (exception being the 3.7-μm band). The diffuse sky albedo is relevant to the cloud retrieval problem. While a continuous yearly product was being processed, it was decided to take a single 16-day dataset (from end of November 2000) and aggregate by land cover type to determine to what extent ecosystem could be used as a predictor of spectral albedo. The MODIS land cover product MOD12 provides a global 1-km IGBP (International Geosphere-Biosphere Programme) land cover classification map for such a study [32]. A tundra ecosystem, not included in the IGBP classification, was added for the study [33]. Separate aggregations were performed by latitude band (tropical, midlatitude, high latitude). Global analysis showed the dispersion in albedo for any given ecosystem to generally be less than 20% (i.e., the ratio of the standard deviation to the mean). A seasonal cycle was derived from hemispheric differences with the assumption that albedos were characteristic of wintertime/summertime values in either hemisphere. For example, southern hemisphere (summertime) spectral albedos for a particular ecosystem were assigned to the same northern hemisphere ecosystem during the northern hemisphere summertime. A sinusoidal fit between the summer/winter extremes was made to complete the seasonal cycle. During operational processing, snow and ice masking is provided by the National Snow and Ice Data Center's Near real-time Ice and Snow Extent (NISE) product [9] with assigned spectral albedos provided from a variety of field measurements [34].

Fig. 5 shows the major ecosystems for the granule being discussed, along with the 1.6-μm diffuse sky albedo for
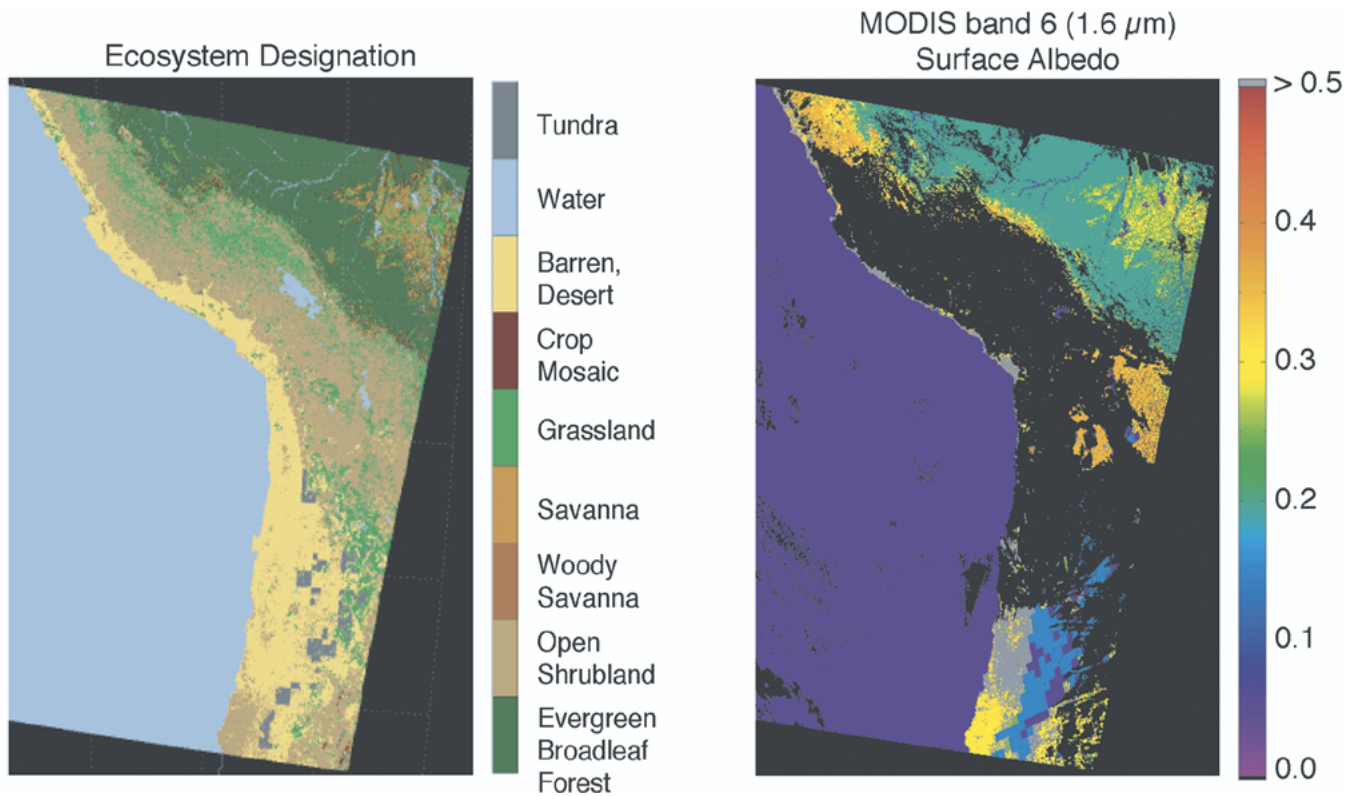
Fig. 5. Ecosystem designation (left panel) determined primarily from MODIS observations (MOD12 product). The ecosystem-based diffuse sky surface albedo for the 1.6-μm MODIS band (right panel) is derived from aggregation of the MODIS albedo product (MOD43) by ecosystem. The derived albedo is only being shown for those pixels where optical and microphysical retrievals are attempted.

those pixels processed by the cloud retrieval algorithm. The east-west change in albedo over the Andes in the southern part of the image is because the region was flagged as having snow/ice by the NISE product and not due to an ecosystem change. The larger albedos in the image are associated with vegetation cover (grasslands/savanna over central Boliva being the largest). Albedos of 0.2 to 0.4 (common) can significantly increase above-cloud reflectance measurements and subsequent retrievals. As an example, consider a liquid water cloud with an optical thickness of 10 and effective radius 10 μm. For a nadir view and solar zenith angle similar to the granule data, a 1.6-μm surface albedo of 0.2 (e.g., "evergreen broadleaf forest," Fig. 5) results in about a 10% relative increase in the above-cloud reflectance compared with an ocean surface; a surface albedo of 0.4 results in about a 20% increase. Note that the Uyuni Salt Flat in not delineated in the ecosystem map.

3) Atmospheric Corrections: For a strictly absorbing atmosphere, the cloud-top reflectance (i.e., in the absence of an atmosphere) is $R_c = R_{\text{TOA}}/t(\mu, \mu_0)$ where R_{TOA} is the measured reflectance at the top of the atmosphere and t is the round-trip or two-way band-averaged transmittance that includes the solar path to cloud top (zenith angle of θ_0) and reflection back toward the satellite (θ). The SWIR/MWIR MODIS bands used in the cloud retrieval algorithm (Table I) can have appreciable water vapor absorption. Water vapor transmittance in these window bands is primarily dependent on the integrated amount of vapor above-cloud and not on the details of the moisture distribution. In other words, the transmittance function can be approximated as $t(\mu, \mu_0, p_c, w(p_c))$, where w is the above-cloud precipitable

water and p_c the cloud-top pressure. Absorption by trace gases may also be important and will similarly depend on p_c.

A library of band-averaged transmittances was calculated using MODTRAN4 [35] for a variety of cloud moisture and temperature profiles, combinations of θ_0 and θ, and selected pressure heights. Mean transmittances and standard deviations for the profiles were catalogued. Typically, the dispersion was on the order of a few percent or less making such a library suitable for cloud retrieval atmospheric corrections. In the cloud retrieval algorithm, the transmittance library is used in conjunction with the MODIS cloud-top pressure product (Section II-B) and integrated water amounts calculated from NCEP GDAS. For the 0.65-μm band (only used for clouds over land), Rayleigh scattering can be important modifier of radiation for thin clouds and for thick clouds at large solar and viewing angles. A Rayleigh correction for this band is implemented using an iterative method [36] that is applied after the absorption correction.

In-cloud gaseous absorption decreases the apparent cloud particle single scattering albedo. This effect on warm and low water cloud effective radius retrievals is estimated [37] to result in errors of about +3.5% when using the 1.6-μm band to about +2.0% for the 2.1- and 3.7-μm bands (nearly independent of actual effective radius). The size error increases with the concentration of water vapor and other gases active in these bands so the effect for cold and high clouds would be less. Ice particles generally have smaller single scattering albedos than water droplets and are therefore less sensitive to gaseous absorption. The maximum expected submicron errors
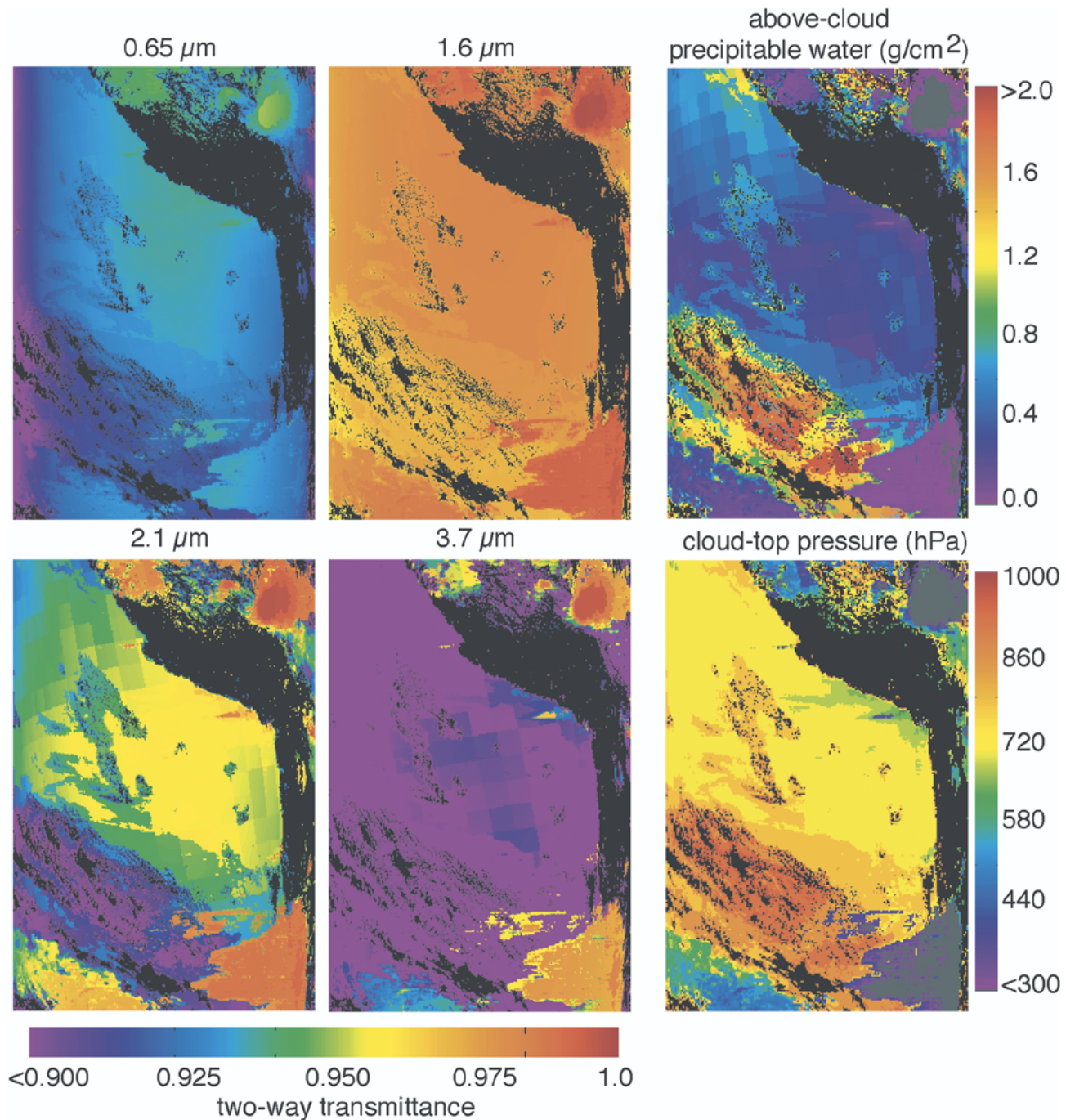
Fig. 6. Two-way band-averaged transmittance for four MODIS bands used in the optical/microphysical retrievals of Figs. 7 and 8 (set of four panels to the left). The transmittance routine requires the integrated above-cloud water amount (upper right panel), which is, in turn, derived from model moisture profile data and the cloud-top pressure field [lower right, cf. Fig. 3(a)].

(e.g., $\sim$0.2 μm for a 10-μm water droplet retrieved with the 2.1-μm band) are ignored. The effect of gaseous absorption beneath the cloud can be approximated by a reduction in the specified surface albedo if the cloud-base height is known and is associated with a single layer cloud system; in the absence of such information this effect is currently ignored.

Two-way spectral transmittances for the granule under discussion are shown in Fig. 6 (unmapped projection) along with the above-cloud column water and cloud-top pressure fields. Absorption in the 0.65-μm band is primarily a result of relatively uniform stratospheric ozone; view angle (swath-sym-

metric) and solar zenith angle variations are seen. All other bands have appreciable water vapor absorption that increases with band central-wavelength. The result is a transmittance pattern that is a function of cloud height and modeled moisture profiles as well as geometry. Note that in some areas of the stratocumulus, the 2.1-μm transmittance can be as low as $\sim$0.9 which means correcting the measured satellite reflectance by the factor 0.90^{-1} ($>$10% increase).

The 3.7-μm band signal includes emitted radiation as well as solar reflectance. The cloud-top temperature product is used to account for the cloud emission component. Atmospheric
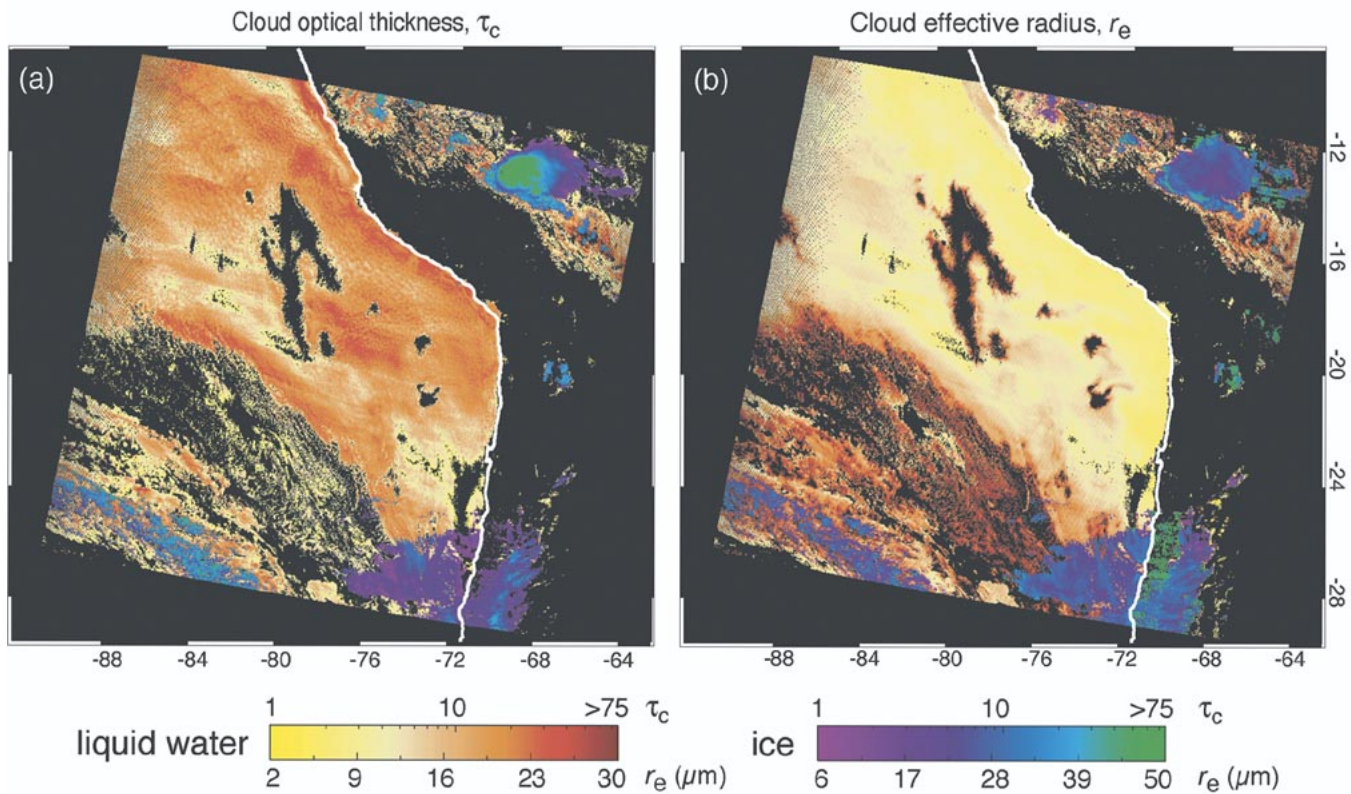
Fig. 7.   (a) Cloud optical thickness and (b) effective particle radius retrievals for the image of Fig. 1, with separate color bars for liquid water and ice clouds. Retrievals use the MODIS 2.1-μm band in conjunction with the 0.65-μm band (over land) and the 0.86-μm band (over water).

emission in the 3.7-μm band can be important for low clouds underlying a wet atmosphere (on the order of 10% of the solar reflectance component for an optically thick water cloud with an effective radius of 10 μm). This atmospheric emission is approximated by a single homogeneous layer having a temperature equal to the above-cloud water-vapor-weighted mean temperature (derived from NCEP water and temperature profiles and the cloud-top pressure product), and an emissivity equal to the above-cloud path absorption in the band (obtained from the transmittance library as previously described). For a variety of cloud-top pressures, water amounts, and profiles, this generally gives atmospheric emission within 20% of exact calculations.

4) Retrievals: The optical thickness and effective radius retrievals are derived from use of a MODIS water-absorbing band (1.6, 2.1, 3.7 μm) in conjunction with one of the nonabsorbing bands (0.65, 0.86, 1.2 μm); the latter primarily provide optical thickness information while absorbing bands contain strong particle size information. The nonabsorbing band is chosen to minimize the underlying surface reflectance; the 0.65-, 0.86-, and 1.2-μm bands are chosen for land, ocean and ice/snow surfaces, respectively. With this choice, three different retrievals are made with the selected nonabsorbing band and each of the absorbing bands. The default retrieval of optical thickness, effective radius, and water path (proportional to the product of the two) uses the 2.1-μm band combination. Particle size retrieved from combinations with the 1.6- and 3.7-μm bands are reported as differences in retrieved effective radius relative to the 2.1-μm band. The optical thicknesses resulting from the three separate retrievals are

similar as they are derived primarily from the common nonabsorbing band that has little sensitivity to particle size.

Fig. 7(a) and (b) shows the 2.1-μm default retrieval with separate color bars for the water and ice phases [Fig. 4(a)]. The stratocumulus water clouds are optically thick (>20) in places, though the convective ice cloud to the north has an optical thickness in excess of ~ 70 in its core. The broken stratocumulus show small optical thickness (1–3) and effective radius in the maximum size range allowable by the water libraries (maximum of up to 30 μm). This low optical thickness and large effective radius is indicative of subpixel cloudiness where clear regions on a subpixel scale reduce the reflectance of what is assumed to be an overcast pixel. A 30-μm retrieval is interpreted as a failed retrieval (e.g., incorrect phase, subpixel cloud, etc.) and the pixel is assigned a fill (null) value for both effective radius and optical thickness. Effective radius retrievals in the 20+-μm range are likely problematic as well and as such are given less weighting in global aggregations (see Section III). Elsewhere, the more uniform cloud deck shows reasonable effective radii of around 10 μm or less through much of the region. The range of effective radii for the ice cloud models lie between 7 and 60 μm. In the northern convection, particle sizes are seen to be relatively small ($\sim$15–20 μm) compared with the surrounding ice cloud $\sim$25–30 μm.

Fig. 8 shows the effective radius difference images. For the liquid water stratocumulus region, $r_{e,1.6} - r_{e,2.1}$ differences are generally within 1 μm but are often biased slightly negative (yellow colors) as expected from parcel theory [38] and in agreement with stratocumulus retrievals from aircraft [27],
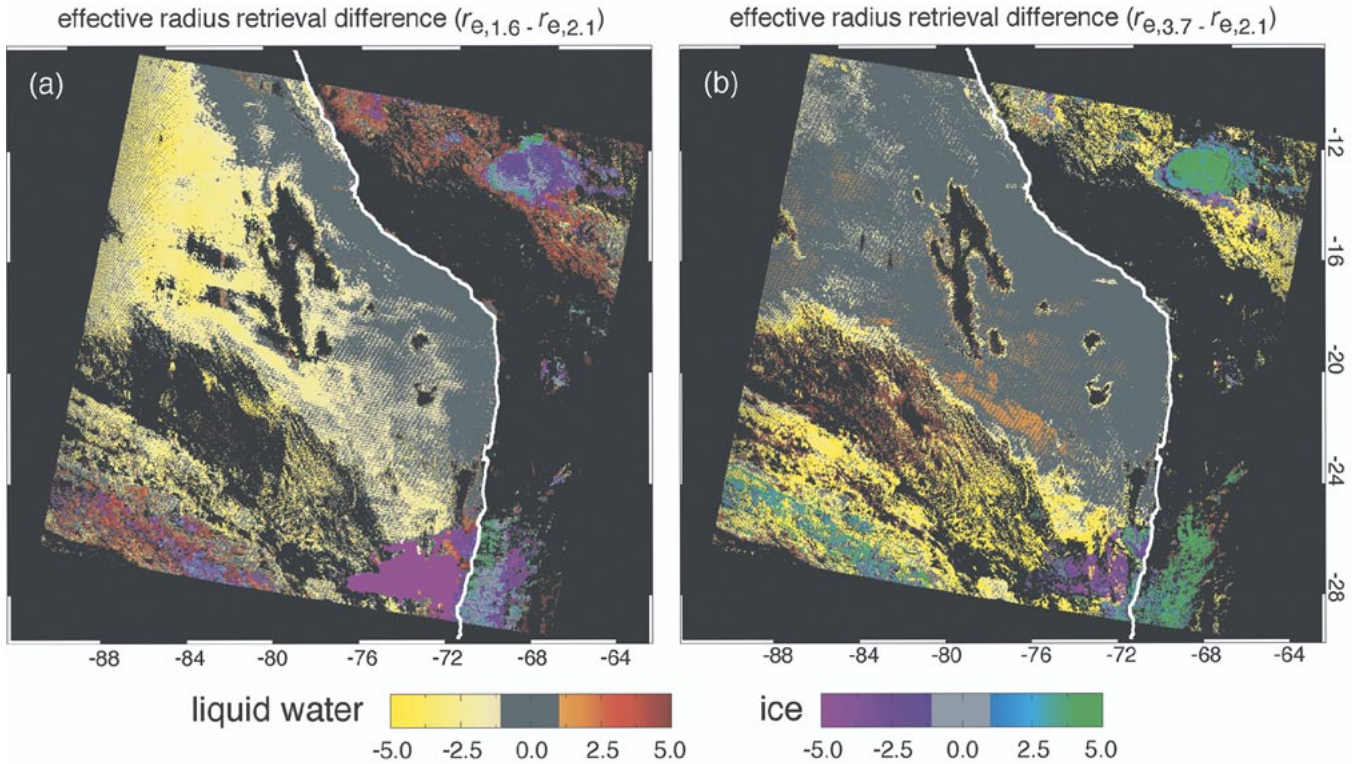
Fig. 8.   Differences in retrieved effective particle radius (micrometer) using the 1.6- and 3.7-μm bands relative to a size retrieval using the 2.1-μm band (Fig. 7(b)).

[28]. In contrast, the $r_{e,3.7} - r_{e,2.1}$ differences are slightly positive for the same region, though typically less than 1 μm (obscured by gray coloration); these differences are somewhat less than the micrometer or so positive differences expected from theory (and in contrast to larger than expected positive differences in the cited aircraft retrievals). The broken stratocumulus region shows substantial negative differences for $r_{e,1.6} - r_{e,2.1}$ and many failures in the 1.6-μm band size retrievals (both fill values and pixels for which no retrieval was attempted are imaged as black). Large differences (positive and negative) are seen for $r_{e,3.7} - r_{e,2.1}$ in the same region. For the thick ice cloud, $r_{e,1.6} - r_{e,2.1}$ differences are negative while $r_{e,3.7} - r_{e,2.1}$ differences are positive and large.

The discussion leading to this example granule retrieval highlights the difficulties and, in particular, the need for ancillary information required for global cloud retrievals. While the example demonstrates progress made toward that end, areas of the algorithm requiring further investigation include the identification of subpixel cloudiness and improvements to ice cloud models (e.g., representative models for a greater variety of cloud types and geographic locations). Current efforts are investigating the use of different spectral band combinations [28], and transitioning from the ecosystem-derived surface albedo map to one based on seasonal MODIS albedo retrievals.

III. GLOBAL-LEVEL CLOUD PRODUCTS

Pixel-level retrievals have a variety of uses including case study and validation efforts. However, global aggregation in both space and time are essential for the development of cloud parameterizations and climate change studies. The Level-3 aggregation of pixel-level (Level-2) retrievals is discussed in a companion paper [1]. We will mention just a few unique aspects of the cloud aggregations.

All MODIS atmosphere products (SDSs) are aggregated at a 1° spatial resolution on a daily, eight-day, and monthly basis. Aggregations include a variety of statistical information (mean, standard deviation, max/min occurrences) and histograms (marginal and joint). As an example, the optical thickness SDS aggregated provides logarithmic mean and standard deviation in addition to linear statistics. The aggregation is given separately for water, ice, and uncertain/mixed phase retrievals. An optical thickness histogram is generated for the water and ice phases. Joint histograms of optical thickness versus effective radius, cloud-top temperature, and effective emissivity are provided for the water and ice phases separately. Similarly, effective radius is binned against cloud-top temperature and effective emissivity.

As discussed in the example from Section II-D-IV, portions of the retrieval space for water clouds (small optical thickness and/or larger effective radius) are, at best, very sensitive to measurement and modeling error, and at worst, indicative of problem retrievals. As such, two separate L3 global aggregations are calculated—unweighted and QA-weighted. For the latter, a *retrieval QA* integer (0 to 3) is assigned to each retrieval and used as the weighting. As both small optical thickness and large particle retrievals are reasonable for ice clouds, these retrievals are given full weighting except when the effective radius retrieval is at the limit of the library space ($\sim$6 and 60 μm).

There is no direct aggregation of the MODIS cloud mask results (aggregation is only made for Level-2 SDSs). However,

there are two sources of cloud fraction available in the Level-3 data file. The cloud-top properties portion of the Level-3 file provides an SDS called "Cloud_Fraction_Infrared" (i.e., derived from the CO_2 IR algorithm) which is an aggregation of the Level-2 MOD06 SDS "Cloud_Fraction." This fraction is simply the counts of *cloudy* and *probably cloudy* outcomes observed during the processing of the cloud-top algorithm. As such, it provides a cloud mask fraction calculation for the two highest confidence cloud bits in the mask. Though the cloud-top properties algorithm is only run when four of the 25 pixels being analyzed at any one time are found to be *cloudy/probably cloudy*, the Cloud_Fraction SDS is populated for all 5×5 pixel groupings. There are also separate day and night cloud fractions SDSs as cloud extent can have a significant diurnal cycle. Further, there is an expected increase in the daytime cloud mask accuracy due to additional information in the solar spectral tests.

The optical/microphysical retrievals also provide a cloud fraction. These are referred to, for example, as "Cloud_Fraction_Water" for the liquid water phase (fraction of ice, uncertain/mixed, and all phases are also provided). These are the number of successful optical/microphysical retrievals normalized by the total number of available pixels (clear and cloudy). However, pixels associated with a failed retrieval outcome during processing are not counted in the normalization as they often represent those pixels that could have been categorized as either clear for cloudy. This fraction is not necessarily the same as the one based on a cloud mask *cloudy/probably cloudy* outcome (e.g., in sunglint, the current decision tree only allows retrievals for the highest confidence cloud mask bit). Further, this fraction is only available for daytime observations.

IV. Summary

This paper has presented an overview of the core pixel-level (Level-2) MODIS operational cloud products. The products consist of a cloud mask for detection of clear skies, cloud-top properties (temperature, pressure, effective emissivity), cloud thermodynamic phase, and cloud optical thickness and microphysical properties (effective radius, water path). An accompanying paper in this issue [1] discusses the global gridded Level-3 datasets. We have highlighted the main features of the algorithms, including retrieval issues and future efforts, via an example data granule (5 min of MODIS data) off the coasts of Peru and Chile. While the example and discussion have featured Terra MODIS, the same algorithms will be applied to Aqua MODIS data. The cloud algorithms have been periodically updated and modified as Terra analysis proceeded. The status of the algorithms and example products described in this paper are valid for the so-called "collection 004" production runs which began in November 2002 for both Terra and Aqua MODIS.

In the course of the discussion, we examined in detail the cloud product pixel-level retrievals over a large-scale region (approximately 2000×2330 km). At the highest available resolution, and without benefit of temporal or spatial averaging, these retrievals demonstrate where we have confidence in the results as well as areas requiring more attention. Features apparent in pixel-level retrieval are not necessarily noticeable in Level-3 or climatological datasets, where random errors may cancel and biases are difficult to discern. Validation of the cloud products, though not discussed in this paper, has been a high priority among the MODIS cloud team members and will continue into the Aqua time frame. A summary document of MODIS atmosphere validation activities is available at *modis-atmos.gsfc.nasa.gov/reference_atbd.html*.

Further details, documentation, example data products, and Level-3 operational imagery can be found at the MODIS atmosphere Web site (*modis-atmos.gsfc.nasa.gov*).

References

[1] M. D. King, W. P. Menzel, Y. J. Kaufman, D. Tanre, B.-C. Gao, S. Platnick, S. A. Ackerman, L. A. Remer, R. Pincus, and P. A. Hubanks, "Cloud and aerosol properties, precipitable water, and profiles of temperature and water vapor from MODIS," *IEEE Trans. Geosci. Remote Sensing*, vol. 41, pp. 442–458, Feb. 2003.

[2] P. A. Ardanuy, D. Han, and V. V. Salomonson, "The Moderate Resolution Imaging Spectrometer (MODIS) science and data system requirements," *IEEE Trans. Geosci. Remote Sensing*, vol. 29, pp. 75–88, Jan. 1991.

[3] M. D. King, Y. J. Kaufman, W. P. Menzel, and D. Tanré, "Remote sensing of cloud, aerosol, and water vapor properties from the Moderate Resolution Imaging Spectrometer (MODIS)," *IEEE Trans. Geosci. Remote Sensing*, vol. 30, pp. 2–27, Jan. 1992.

[4] W. L. Barnes, T. S. Pagano, and V. V. Salomonson, "Prelaunch characteristics of the 'Moderate Resolution Imaging Spectroradiometer (MODIS) on EOS-AM1," *IEEE Trans. Geosci. Remote Sensing*, vol. 36, pp. 1088–1100, July 1998.

[5] J. J. Butler and R. A. Barnes, "Calibration strategy for the Earth Observing System (EOS)-AM1 platform," *IEEE Trans. Geosci. Remote Sensing*, vol. 36, pp. 1056–1061, July 1998.

[6] B. Guenther, G. D. Godden, X. Xiong, E. J. Knight, S. Y. Qiu, H. Montgomery, M. M. Hopkins, M. G. Khayat, and Z. Hao, "Prelaunch algorithm and data format for the level 1 calibration products for the EOS-AM1 Moderate Resolution Imaging Spectroradiometer (MODIS)," *IEEE Trans. Geosci. Remote Sensing*, vol. 36, pp. 1142–1151, July 1998.

[7] A. Slingo and H. M. Schrecker, "On the shortwave radiative properties of stratiform water clouds," *Q. J. R. Meteorol. Soc.*, vol. 108, pp. 407–426, 1982.

[8] S. A. Ackerman, K. I. Strabala, W. P. Menzel, R. A. Frey, C. C. Moeller, and L. E. Gumley, "Discriminating clear-sky from clouds with MODIS," *J. Geophys. Res.*, vol. 103, pp. 32 141–32 158, 1998.

[9] R. L. Armstrong and M. J. Brodzik, "Recent northern hemisphere snow extent: A comparison of data derived from visible and microwave satellite sensors," *Geophys. Res. Lett.*, vol. 28, pp. 3673–3676, 2001.

[10] R. W. Grumbine, "Automated passive microwave sea ice concentration aalysis at NCEP," NOAA, DOC/NOAA/NWS/NCEP/EMC/OMB Tech. Note 120, 1996.

[11] W. P. Menzel, W. L. Smith, and T. R. Stewart, "Improved cloud motion wind vector and altitude assignment using VAS," *J. Appl. Meteorol.*, vol. 22, pp. 377–384, 1983.

[12] D. P. Wylie and W. P. Menzel, "Eight years of high cloud statistics using HIRS," *J. Climate*, vol. 12, pp. 170–184, 1999.

[13] J. C. Derber, D. F. Parrish, and S. J. Lord, "The new global operational analysis system at the National Meteorological Center," *Weather Forecasting*, vol. 6, pp. 538–547, 1991.

[14] B. A. Wielicki and J. A. Coakley Jr, "Cloud retrieval using infrared sounder data: Error analysis," *J. Appl. Meteorol.*, vol. 20, pp. 157–169, 1981.

[15] W. P. Menzel, D. P. Wylie, and K. I. Strabala, "Seasonal and diurnal changes in cirrus clouds as seen in four years of observations with the VAS," *J. Appl. Meteorol.*, vol. 31, pp. 370–385, 1992.

[16] B. A. Baum and B. A. Wielicki, "Cirrus cloud retrieval using infrared sounding data: Multilevel cloud errors," *J. Appl. Meteorol.*, vol. 33, pp. 107–117, 1994.

[17] W. R. Reynolds and T. M. Smith, "Improved global sea surface temperature analyses using optimum interpolation," *J. Climate*, vol. 7, pp. 929–948, 1994.

[18] K. I. Strabala, S. A. Ackerman, and W. P. Menzel, "Cloud properties inferred from 8–12 μm data," *J. Appl. Meteorol.*, vol. 2, pp. 212–229, 1994.

[19] B. A. Baum, P. F. Soulen, K. I. Strabala, M. D. King, S. A. Ackerman, and W. P. Menzel, "Remote sensing of cloud properties using MODIS airborne simulator imagery during SUCCESS, 2, cloud thermodynamic phase," *J. Geophys. Res.*, vol. 105, pp. 11 781–11 792, 2000.

[20] B. A. Baum, D. P. Kratz, P. Yang, S. C. Out, Y. Hu, P. F. Soulen, and S. C. Tsay, "Remote sensing of cloud properties using MODIS airborne simulator imagery during SUCCESS, 1, data and models," *J. Geophys. Res.*, vol. 105, pp. 11 767–11 780, 2000.

[21] S. Twomey and T. Cocks, "Spectral reflectance of clouds in the near-infrared: Comparison of measurements and calculations," *J. Meteorol. Soc. Jpn.*, vol. 60, pp. 583–592, 1982.

[22] A. Arking and J. D. Childs, "Retrieval of cloud cover parameters from multispectral satellite images," *J. Climate Appl. Meteorol.*, vol. 24, pp. 322–333, 1985.

[23] T. Nakajima and M. D. King, "Determinations of the optical thickness and effective particle radius of clouds from reflected solar radiation measurements. Part I: Theory," *J. Atmos. Sci.*, vol. 47, pp. 1878–1893, 1990.

[24] F. Rawlins and J. S. Foot, "Remotely sensed measurements of stratocumulus properties during FIRE using the C130 aircraft multichannel radiometer," *J. Atmos. Sci.*, vol. 47, pp. 2488–2503, 1990.

[25] S. Platnick and S. Twomey, "Determining the susceptibility of cloud albedo to changes in droplet concentrations with the Advanced Very High Resolution Radiometer," *J. Appl. Meteorol.*, vol. 33, pp. 334–347, 1994.

[26] Q. Han, W. B. Rossow, and A. A. Lacis, "Near-global survey of effective droplet radii in liquid water clouds using ISCCP data," *J. Climate*, vol. 7, pp. 465–497, 1994.

[27] S. Platnick, P. A. Durkee, K. Nielsen, J. P. Taylor, S. C. Tsay, M. D. King, R. J. Ferek, P. V. Hobbs, and J. W. Rottman, "The role of background cloud microphysics in the radiative formation of ship tracks," *J. Atmos. Sci.*, vol. 57, pp. 2607–2624, 2000.

[28] S. Platnick, J. Y. Li, M. D. King, H. Gerber, and P. V. Hobbs, "A solar reflectance method for retrieving the optical thickness and droplet size of liquid water clouds over snow and ice surfaces," *J. Geophys. Res.*, vol. 106, pp. 15 185–15 199, 2001.

[29] P. Yang and K. N. Liou, "Finite-difference time domain method for light scattering by small ice crystals in three-dimensional space," *J. Opt. Soc. Amer.*, vol. 13, pp. 2072–2085, 1996.

[30] ——, "Geometric optics integral equation method for light scattering by nonspherical ice crystals," *Appl. Opt.*, vol. 35, pp. 6568–6584, 1996.

[31] W. Lucht, C. B. Schaaf, and A. H. Strahler, "An algorithm for the retrieval of albedo from space using semiempirical BRDF models," *IEEE Trans. Geosci. Remote Sensing*, vol. 38, pp. 977–998, Mar. 2000.

[32] M. A. Friedl, D. Muchoney, D. McIver, F. Gao, J. C. F. Hodges, and A. H. Strahler, "Characterization of North American land cover from NOAA-AVHRR data using the EOS MODIS land cover classification algorithm," *Geophys. Res. Lett.*, vol. 27, p. 977, 2000.

[33] J. S. Olson, J. A. Watts, and L. J. Allison, "Carbon in live vegetation of major world ecosystems," Environmental Sci. Div., Oak Ridge National Lab., Oak Ridge, TN, ORNL-5862, 1983.

[34] G. T. Arnold, S. C. Tsay, M. D. King, J. Y. Li, and P. F. Soulen, "Airborne spectral measurements of surface-atmosphere anistotropy for Arctic sea ice and tundra," *Int. J. Remote Sens.*, vol. 23, pp. 3763–3781, 2002.

[35] A. Berk, L. S. Bernstein, G. P. Anderson, P. K. Acharya, D. C. Robertson, J. H. Chetwynd, and S. M. Adler-Golden, "MODTRAN cloud and multiple scattering upgrades with application to AVIRIS," *Remote Sens. Environ.*, vol. 65, pp. 367–375, 1998.

[36] M. Wang and M. D. King, "Correction of Rayleigh scattering effects in cloud optical thickness retrievals," *J. Geophys. Res.*, vol. 102, pp. 25 915–25 926, 1997.

[37] S. Platnick and F. P. J. Valero, "A validation of a satellite cloud retrieval during ASTEX," *J. Atmos. Sci.*, vol. 52, pp. 2985–3001, 1995.

[38] S. Platnick, "Vertical photon transport in cloud remote sensing problems," *J. Geophys. Res.*, vol. 105, pp. 22 919–22 935, 2000.

Steven Platnick received the B.S. degree in electrical engineering from Duke University, Durham, NC, in 1979, the M.S. degree in electrical engineering from the University of California, Berkeley, in 1980, and the Ph.D. degree in atmospheric sciences from the University of Arizona, Tucson, in 1991.

He has worked in collaboration with NASA Goddard Space Flight Center, Greenbelt, MD, since 1993, most recently as a member of the Laboratory for Atmospheres and prior to that as a Research Associate Professor with the Joint Center for Earth Systems Technology, University of Maryland—Baltimore County, Baltimore, from 1996-2002. He was a National Research Council Resident Research Associate at NASA Ames Research Center, Moffett Field, CA from 1991 to 1993 and held engineering positions at Hewlett-Packard Co., Santa Rosa, CA from 1981-1987. His research experience includes theoretical and experimental studies of satellite, aircraft, and ground-based cloud remote sensing, including applications to MODIS. He is an Associate Member of the MODIS Science Team.
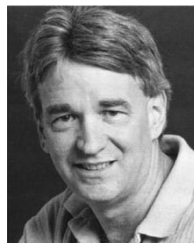
Michael D. King (M'01) received the B.A. degree in physics from Colorado College, Colorado Springs, in 1971, and the M.S. and Ph.D. degrees in atmospheric sciences from the University of Arizona, Tucson, in 1973 and 1977, respectively.

In January 1978, he joined NASA Goddard Space Flight Center and is currently Senior Project Scientist of NASA's Earth Observing System (EOS), a position he has held since 1992. He is a member of the MODIS Science Team where he has primary responsibility for developing the cloud optical and microphysical property and Level-3 algorithms. His research experience includes conceiving, developing, and operating multispectral scanning radiometers from a number of aircraft platforms in field experiments ranging from arctic stratus clouds to smoke from the Kuwait oil fires in the Persian Gulf and biomass burning in Brazil and southern Africa.

Dr. King is a member of the U.S. National Academy of Engineering.

Steven A. Ackerman received the Ph.D. degree in atmospheric sciences from Colorado State University, Fort Collins, in 1987.

He joined the faculty of the Department of Atmospheric and Oceanic Sciences, University of Wisconsin, Madison, in 1992, where he is currently a Professor. He is also the Director of the Cooperative Institute for Meteorological Satellite Studies, Madison, WI, a position he has held since 1999. He is an Associate Member of the MODIS Science Team where he has primary responsibility for the MODIS cloud mask algorithm. His research experience includes remote sensing, radiative transfer, earth radiation budgets, cloud radiative parameterizations, climate change, and aerosol studies. In addition to his participation in the MODIS Science Team, he is responsible for the cloud mask algorithm on the Global Imager (GLI), a sensor on Japan's ADEOS II spacecraft.

W. Paul Menzel received the B.S. degree in physics from the University of Maryland, College Park, in 1967, and the M.S. and Ph.D. degrees in theoretical solid-state physics from the University of Wisconsin, Madison, in 1968 and 1974, respectively.

In 1975, he joined the Space Science and Engineering Center, University of Wisconsin, where he was among the first to explore the possibilities for remote sensing of earth's atmosphere from a geosynchronous satellite. In 1983, he joined the National Oceanic and Atmospheric Administration National Environmental Satellite, Data, and Information Service (NOAA/NESDIS) to head the Advanced Satellite Products Project, where he was responsible for the development, testing, and evaluation of procedures for deriving new atmospheric products from spaceborne observations, and along with their transfer from the research laboratory to the operational weather forecaster. He is currently the Chief Scientist of the Office of Research and Applications of NOAA/NESDIS. He is also a member of the MODIS Science Team, where he has primary responsibility for algorithms to derive cloud-top properties, atmospheric profiles, and column water vapor using infrared bands on MODIS.

Bryan A. Baum received the Ph.D. degree in atmospheric sciences from the Georgia Institute of Technology, Atlanta, GA, in 1989.

He is a Senior Research Scientist with the Radiation and Aerosols Branch, NASA Langley Research Center (LaRC), Hampton, VA, but is stationed at the Cooperative Institute for Meteorological Satellite Studies, University of Wisconsin (UW), Madison. He is an Adjunct Professor with the Department of Atmospheric and Oceanic Science, UW-Madison. Research activities have focused on satellite-, aircraft-, and surface-based remote sensing of multilayered cloud properties from multispectral imagery, global cloud retrievals derived from satellite data, global fire and smoke detection, and the effect of clouds and aerosols on earth's radiation budget.

Jérôme C. Riédi received the B.S. degree in physics and the M.S. and Ph.D. degrees in atmospheric sciences in 1997, 1998, and 2001, respectively, all from the University of Lille, Villeneuve d'Ascq, France. His doctoral research included the use of multiangle and polarization measurements from the Polarization and Directionality of the Earth's Reflectances/Advanced Earth Observation Satellite for determination of cloud microphysical properties.

In 2001, he came to NASA Goddard Space Flight Center, Greenbelt, MD, where he is currently a Research Associate with the Goddard Earth Science and Technology Center, University of Maryland—Baltimore County, Baltimore. His research interests focus on the remote sensing of cloud properties using passive measurements from satellite and airborne instruments in the visible and infrared region of the spectrum. He is currently involved in the Moderate Resolution Imaging Spectroradiometer (MODIS) and MODIS Airborne Simulator (MAS) cloud thermodynamic phase retrieval algorithms and quality assessment of the cloud optical and microphysical retrieval products.

Richard A. Frey received the B.S. degree in meteorology from Millersville University of Pennsylvania, MIllersville, in 1986, and the M.S. degree in meteorology from the University of Wisconsin, Madison, in 1988.

He is currently an Associate Researcher with the Cooperative Institute for Meteorological Satellite Studies, Madison, WI.